EPJ Photovoltaics **16**, 14 (2025)

https://doi.org/10.1051/epjpv/2025001

Available online at:
www.epj-pv.org

Special Issue on 'EU PVSEC 2024: State of the Art and Developments in Photovoltaics', edited by Robert Kenny and Gabriele Eder

ORIGINAL ARTICLE OPEN ACCESS

Enhancing fault diagnosis in photovoltaic plants: managing the simultaneity of faulty bypass diodes, series resistance increases, and partial shading effects

Giosue' Maugeri[1,*], Simone Arrigoni[1], Alessandro Lavelli[2], Davide Bombelli[1], Salvatore Guastella[1], Andrea Rossetti[1], and Marcello Restelli[2,3]

[1] Ricerca sul Sistema Energetico – RSE SpA, via R. Rubattino 54, 20134 Milan, Italy
[2] ML cube, via Rosso di San Secondo 1/3, 20134 Milan, Italy
[3] Politecnico di Milano – Dipartimento di Elettronica, Informazione e Bioingegneria, piazza Leonardo da Vinci 32, 20133 Milan, Italy

Received: 13 September 2024 / Accepted: 6 January 2025

Abstract. Modern photovoltaic (PV) monitoring systems can collect high-quality data; however, existing analysis tools need to evolve not only to identify yield issues but also to discern the nature of faults and degradation factors contributing to yield loss. Current AI-based Operation & Maintenance (O&M) tools primarily focus on detecting single faults, with their accuracy in fault recognizing, significantly diminishing in the presence of multiple concurrent issues. Consequently, diagnostics become unreliable when faults occur alongside other component failures or overlap with environmental effects. The lack of appropriately labelled data for training and validating AI-based tools is a critical weakness that impedes the rapid development of reliable diagnostic solutions. This study introduces a methodology designed to enhance the capability of machine learning (ML) algorithms in identifying and classifying faults, particularly under conditions where multiple failures or environmental effects occur simultaneously. Leveraging the RSE Fault Test Facility, which can replicate a variety of failure modes in real PV systems, we were able to generate over 1.6 million fault-labelled records across more than four years of diverse failure conditions. This study focuses specifically on combined faults scenarios involving short-circuited diodes, increased series resistance and shading effects, with a total of 32,806 labelled records of combined faults. The findings of the study provide a methodology foundation for the development of advanced fault detection and diagnosis tools, aiming to improve their reliability and performance when dealing with the simultaneous occurrence of the aforementioned faults.

Keywords: PV fault diagnosis / AI-based OM / PV reliability / fault-labelled data / PV monitoring / yield loss identification

1 Introduction

Globally, photovoltaic (PV) energy systems continue to rank among the most cost-effective reliable and rapidly expanding technologies for electricity generation. In 2023, solar PV alone accounted for three-quarters of the world's renewable capacity additions. The expansion of renewable electricity capacity is expected to persist over the next five years, driven predominantly by solar PV, which benefits from lower generation costs compared to both fossil and non-fossil alternatives in most countries, and, in some cases, this is combined with support policies; furthermore, PV are high reliable, locally available and free of climate-altering emissions. Solar PV additions are projected to more than double by 2028 compared to 2022, reaching nearly 500 GW over the forecast period [1]. While new PV installations play a significant role in achieving global environmental goals, it is equally important that both existing and new PV systems maintain their reliability and energy performance throughout their operational lifespan without increasing the Levelized Cost of Energy (LCOE). The PV rapid expansion to gigawatt-scale portfolios presents a challenge for PV system operators: the need to quickly train and deploy skilled human resources to effectively manage these large portfolios. Simultaneously, this growth highlights the critical need for continuous innovation and digitalization in the solar PV sector to enhance competitiveness and realize its socio-economic benefits [2].

* e-mail: giosue.maugeri@rse-web.it

Ongoing innovations in PV plant Operation and Maintenance (O&M), particularly in the digitization of information, in the automation of inspections, and in the automated fault detection and diagnosis, are essential for optimizing O&M activities since they can significantly reduce costs. Modern PV monitoring systems that can collect granular and high-quality data offer the possibility to have extensive insights into the performance status of PV plants. Data analysis tools can detect in a prompt way underperformance patterns and alert the PV operators. However, these data analysis tools must evolve to not only recognize yield problems but also identify the nature of faults and other degradation factors that contribute to yield loss, especially in the context of managing gigawatt-scale portfolios. To this purpose, the use of AI-based tools is increasingly attracting the attention of PV operators and investors as they have already shown considerable benefits across various sectors improving process monitoring effectiveness, quickly restoring nominal operating conditions, and reducing the risk of minor faults escalating into more severe issues. In the PV sector, for example, fault detection and diagnosis tools can provide valuable information for O&M operators, enabling them to address issues promptly and optimize repair time and costs. This is especially advantageous for large PV systems, as it positively impacts the LCOE. In recent years, numerous methods for detecting and diagnosing specific faults in photovoltaic systems have been proposed in the literature. Some methods, based on expert-developed statistical rules, focus on fault identification by analysing discrepancies between predicted and actual field measurements [3]. More advanced approaches leverage Deep Learning (DL) techniques. However, a key limitation of current AI-driven maintenance tools is their primary focus on detecting single faults, with accuracy significantly declining in the presence of multiple concurrent issues [4]. The reliability of fault diagnoses in PV systems is often compromised when faults overlap with other component failures or environmental effects. The development of robust models for fault detection and diagnosis is further hampered by the limited availability of historical production datasets from PV plants, which are crucial for the training and validation of machine learning (ML) algorithms. This study addresses these critical challenges by proposing a novel methodology designed to enhance fault diagnosis capabilities in photovoltaic systems. The methodology leverages an experimental setup at the RSE PV Laboratory, specifically the RSE PV Failure Test Facility, which enables the systematic collection and analysis of data. Over a four-year period, this facility has generated a comprehensive PV dataset encompassing over 1.6 million records, each labelled with specific fault events. This extensive dataset allows for a detailed examination of the behaviour of electrical parameters under controlled fault conditions, across varying weather contexts, and in real-world scenarios where additional issues such as data acquisition malfunctions, sensor errors, and seasonal shading effects may arise. These real-world factors are often overlooked in studies that rely solely on data generated by theoretical models. Our research provides detailed guidelines for data processing, with the goal of enhancing the effectiveness of diagnostic algorithms in detecting faults, particularly in complex scenarios where multiple concurrent issues are present within a PV plant. This work represents a significant step forward in the development of reliable fault detection and diagnosis algorithms for photovoltaic systems.

2 Overview of photovoltaic system faults

Photovoltaic (PV) systems are susceptible to a range of faults and malfunctions that can lead to significant losses in output power [5]. The primary components at risk include photovoltaic modules, inverters, mounting structures, cables, connectors, and monitoring systems. Each component is prone to different types of faults, each of which can manifest with distinct observable effects. In particular:

- PV Modules may experience issues such as damaged cells, degradation phenomena, disconnected electrical connections, or fractures in the protective glass [6].
- Inverters may fail due to internal electronic components, which can lead to either a complete halt in electricity production or a significant reduction in conversion efficiency.
- Mounting Structures may face ground subsidence or adverse weather conditions that cause the collapse of the support structures for PV modules; for trackers, faults might involve the failure to accurately follow the sun's movement throughout the day.
- Cables and Connections can deteriorate due to prolonged exposure to environmental factors or, in some cases, prematurely due to improper installation.
- Monitoring and Control Systems could experience interruptions in the acquisition of electrical measurements in the field or errors in reading electrical parameters due to instrumentation not being periodically calibrated.

A list of possible failures is illustrated in Figure 1 where schematically is represented a photovoltaic system with highlights on the main types of faults for each section. A short description of these faults follows.

- **Bypass Diode Failure (A):** this is generally due to continuous thermal and electrical stress. The presence of short-circuited diodes leads to reduced energy performance of the PV system.
- **Line-to-Line Fault (B):** this occurs when there is accidental contact between two points of different potential in a PV string, often due to cable insulation damage or corrosion and water infiltration in field panels. L-to-L faults cause a string voltage mismatch, leading to overcurrent in the affected string, which could be substantial enough to damage the modules and conductors [7].
- **Open circuit Fault (C):** this fault is characterized by the inability of current to flow, resulting in no power output. It is often caused by electrical arc events, broken cells, damaged interconnections, loose connections, or defective power cables due to aging. Frequent plugging and unplugging can also lead to open-circuited terminals [8].

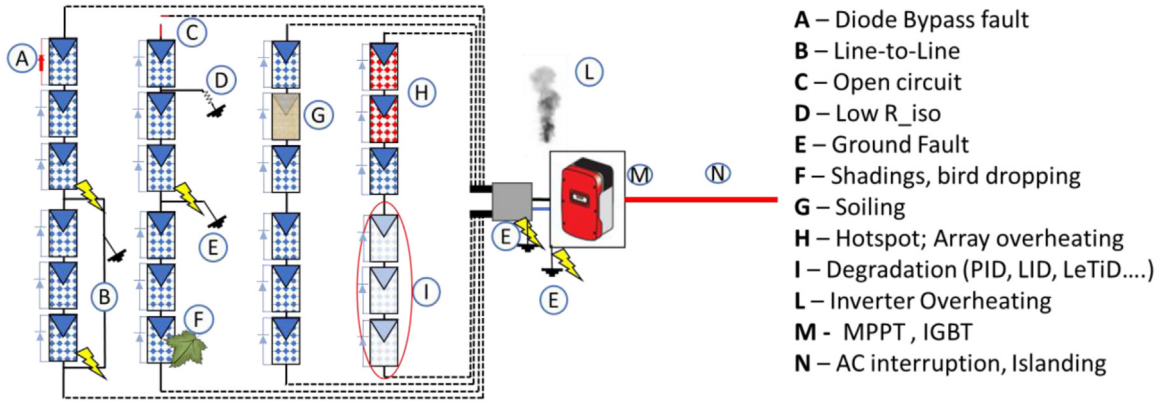

Fig. 1. Schematic representation of a photovoltaic system and main types of faults.

- **Low Insulation Resistance (D):** this fault is typically due to the degradation of the silicone in the junction box of one or more modules within a string, leading to water or moisture infiltration, or due to moisture presence in field panels or string combiner boxes. It may also result from the deterioration of the electrical insulation of cables and connectors. When insulation resistance drops below a preset threshold (around 1 MΩ), the inverter triggers a "Riso Low" alarm, which may lead to disconnection from the grid depending on the inverter's logic.
- **Ground Faults (E):** these occur due to current leakage to the ground on either the DC or AC side, which can manifest within the inverter or the DC section of the system. They are often caused by neglected maintenance of the system's insulation resistance or accidental contact between live parts and the metallic structure of the system.
- **Temporary Daily Shading (F):** this can be systematic, occurring daily or seasonally, with shading typically visible only during certain hours or months of the year (e.g., autumn and winter when the sun's elevation is lower). It can be caused by nearby obstacles (e.g., poles), vegetation (e.g., growing trees and wild plants), or localized soiling (e.g., bird droppings).
- **Soiling (G):** caused by the accumulation of dust/dirt on the module surface. This is a highly variable phenomenon influenced by environmental pollutants, which differ by geographic area. Soiling is also affected by the structural configuration of the PV field, such as module tilt angle, and by the maintenance strategy employed.
- **Hotspot (H):** caused by one or more cell that are forced to operate in reverse polarisation, or by resistive interconnections, or an overheating near the junction box.
- **Array Overheating (H):** generally caused by poor ventilation of PV modules, leading to a temperature mismatch along the PV string.
- **Increased Series Resistance in Modules/Strings (I):** often caused by degradation phenomena in the module cells, such as corrosion of the top and bottom metallic contacts. In a PV string, the Rs value is higher because degradation effects in each module accumulate with the resistances of the interposed contacts along the current path.
- **Potential Induced Degradation – PID (I):** a degradation phenomenon in crystalline silicon PV modules that can occur under high DC voltage, especially in long series-connected PV module strings. It leads to substantial energy production losses (up to several percentage points) and a reduction in the open-circuit voltage of the PV module. Since shunt resistance (RSH) is highly sensitive to PID, monitoring RSH via IV curve measurements can detect the early stages of this phenomenon.
- **Inverter Overheating (L):** this can result from obstructions or failures in the inverter's cooling system or improper placement. Overheating is a major cause of reduced DC/AC conversion efficiency.
- **MPPT fault (M):** the Maximum Power Point Tracking (MPPT) works in conjunction with sensors and charge controllers to identify the maximum power point on the Current-Voltage (I–V) curve of the PV string modules. However, if sensors become disconnected or defective, or if the MPPT algorithm encounters an error, the MPPT zone within the PV system can malfunction, leading to faulty operation [9].
- **AC interruption (N):** it can occur due to damaged connectors between the inverter and its electrical panel, usually due to wear, moisture, or improper installation. Additionally, inverter overload can lead to a shutdown as a protective measure. Faulty fuses or circuit breakers may cause disconnections after short circuits or overloads.

This work, will specifically focus on diagnosing faults related to increased series resistance (RS) at the module/string level, bypass diode failure and partial shading effects on the PV string. This focus is based on previous findings from a study conducted by RSE [10], which highlighted the challenges of accurately diagnosing these faults when they occur simultaneously with others.

3 Classification of faults in photovoltaic systems

The Failure Mode Effect Analysis (FMEA) [11] is a widely used methodology for classifying failure events according to their severity and likelihood of occurrence. This method

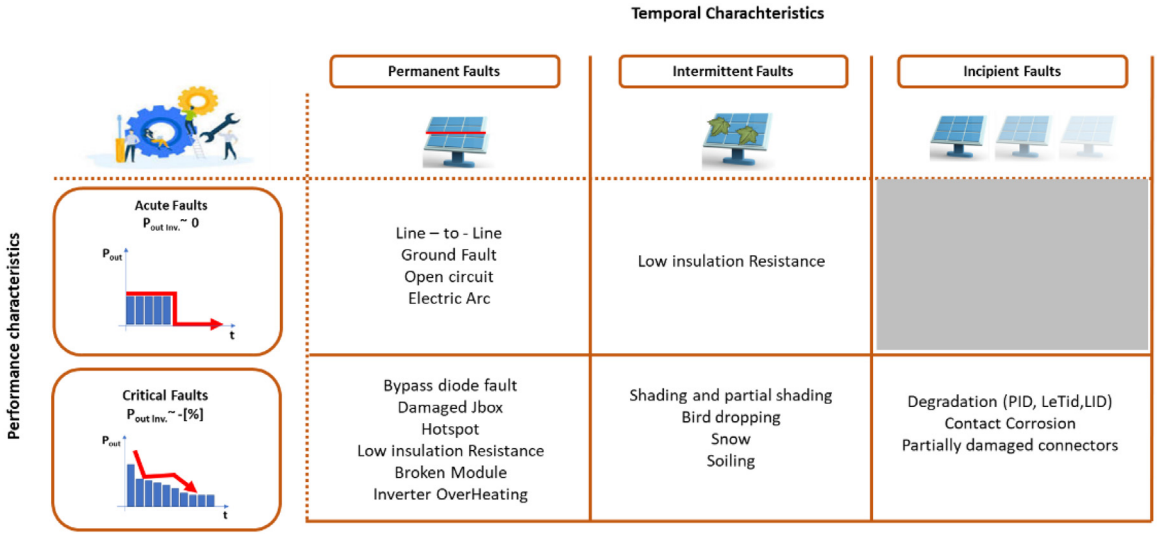

Fig. 2. Fault classification matrix based on temporal and performances characteristics.

enables an objective comparison of various faults and facilitates the prioritization of interventions to mitigate the risks of plant downtime. Once the risks have been identified, appropriate *preventive* measures can be established to address the identified issues. These analyses are periodically conducted by industry experts to refine fault statistics, thereby increasing their accuracy and evaluating the performance of emerging technologies. While this approach is effective for comparing different faults and establishing priorities for fault identification and preventive maintenance, it is limited in providing a practical classification system for recognizing faults based on their observable effects on commonly monitored parameters. To enhance the development of fault diagnostic software tools, a resumption of fault categorization based on their impact on power output [4] and their temporal characteristics [12] is presented below.

3.1 Classification of photovoltaic system faults by power output characteristics

Faults in photovoltaic (PV) systems can be effectively categorized based on their impact on power output, offering valuable insights into the nature and severity of the malfunction. A rapid and noticeable decrease in output power relative to the expected performance typically indicates an acute malfunction, which is generally straightforward to identify. However, not all malfunctions manifest so conspicuously; in many cases, the effects may not be immediately apparent. In such scenarios, advanced data processing techniques become essential for detecting faults or underlying degradation factors.

Based on these characteristics, we categorize faults into acute and critical types:

- **Acute faults** are those whose effects are immediately visible to the PV operator, often leading to a complete loss of power output at the inverter. Common examples of acute faults include ground faults, short circuits, and open circuits. These faults necessitate prompt intervention to prevent total system failure.
- **Critical faults**, on the other hand, are characterized by less immediately apparent effects, which, if unaddressed, can lead to significant energy losses over time. Examples of critical faults include partial shading, bypass diode failures, hotspot formation, degradation-related issues, and soiling. While these faults may initially cause only minor reductions in power output, their cumulative impact can be substantial. This makes sophisticated diagnostic and monitoring strategies essential to ensure timely detection and effective mitigation.

3.2 Classification of photovoltaic system faults by temporal characteristics

In addition to their direct impact on the power output of photovoltaic (PV) systems, faults can be systematically categorized based on their temporal characteristics: permanent, intermittent, and incipient.

- **Permanent faults** typically result from component failures that necessitate on-site technical intervention to restore normal system functionality. Common examples include short circuits, open circuits, and physical damage to junction boxes and connectors [13]. These types of faults lead to sustained performance degradation and require immediate attention to prevent further system deterioration.
- **Intermittent faults**, in contrast, are characterized by their irregular and often unpredictable effects over time. These faults may resolve spontaneously or may be mitigated without the need for on-site intervention. Typical examples include shading (including partial shading), the deposition of bird droppings, and environmental stresses such as dust accumulation, snow buildup, and high humidity. The sporadic nature of these faults can complicate diagnosis and often leads to temporary but significant reductions in power output.
- **Incipient faults** are those that initially exhibit minimal impact but progressively worsen over time due to underlying degradation processes. Such faults are

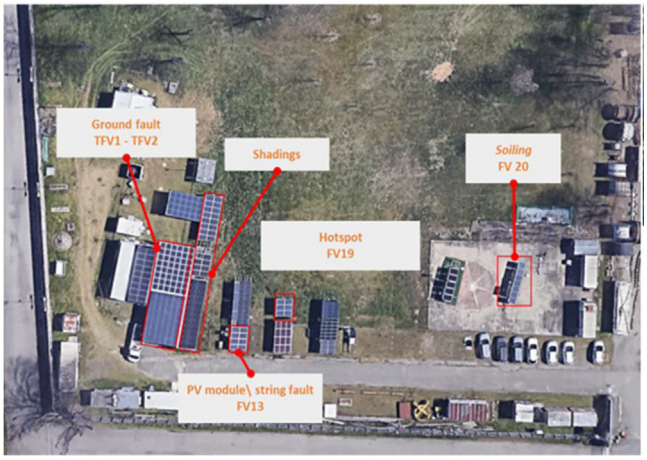

Fig. 3. The RSE PV Fault Facility.

frequently associated with the gradual degradation of PV cells or the corrosion of metallic contacts within PV modules and interconnections. If not identified and addressed early, incipient faults can evolve into permanent failures, ultimately compromising the long-term reliability and efficiency of the PV system.

The description so far can be represented in a matrix that correlates the effects on output power with the temporal characteristics of the faults, as illustrated in Figure 2. Understanding the fault effects on monitored electrical parameters, and their temporal behaviour allow for the development of appropriate data analysis methodologies that can be integrated into mathematical models for fault detection and diagnosis (or fault recognition). Certainly, these models are not intended to replace the necessary protection against specific faults that can present significant safety risks to humans if not properly managed through appropriate design and maintenance criteria for photovoltaic systems, such as low insulation resistance, electrical arc faults, or ground faults. For these risks, it remains crucial to adhere to international standards, such as, IEC 61730 [14] and IEC 60364-7-712 [15], to ensure adequate protection against potential hazards, rather than relying solely on monitoring systems.

The following paragraph describes the hardware setup used for the analysis of the failure effects in the main electrical parameters monitored from a PV system.

4 PV field data available

4.1 PV systems characteristics

The PV data analyzed in this study were generated in the PV Fault Facility of the RSE PV Lab in Milan (Fig. 3) [16]. This facility consists of PV systems equipped with a SCADA system that records data at one-minute intervals, as well as of experimental hardware capable of emulating various fault modes. The electrical characteristics of the PV systems used in this study, along with the specific types of faults that can be reproduced in each system, are detailed in Table 1.

This facility enables the creation of labelled datasets essential for training fault detection models. Over the past four years, it has allowed us to generate over 1.6 million fault-labelled records, with the type of faults listed in Table 1. The dataset continues to grow. Since this work focuses on three types of faults – shorted bypass diodes, increased series resistance, and partial shading – and their simultaneity, we analysed a subset of these labelled records. The following paragraphs describe the experimental setup used for fault replication in the PV System TFV1 and TFV3.

4.2 Monitoring and data logging in PV fault facility operations

The generated PV data are archived in a local database, closely associated with a Test Log maintained for each PV system in the Fault Facility. This log documents test configurations, fault start, and end dates, including a notes section where operators can record pertinent details, such as AC grid interruptions not directly related to the fault condition.

For each PV system, the following parameters were monitored:

- Vdc [V]: String DC voltage
- Idc [A]: String DC current
- Pdc [kW]: String DC power
- Vac [V]: AC grid voltage
- Iac [A]: AC current at inverter output
- Pac [kW]: AC power at inverter output
- Tamb [°C]: Environmental temperature
- Tmod [°C]: Rear module temperature
- IrrPoA [W/m^2]: Plane of Array irradiance
- f [Hz]: Grid frequency
- Tinv [°C]: Inverter temperature.

4.3 Experimental hardware setup

4.3.1 Increased Series resistance and shorted bypass diode

The PV system TFV1, is equipped with an electrical panel (named QFVG-M) specifically designed to replicate faults associated with the progressive increase in series resistance of modules or strings – which can be indicative of gradual degradation within the PV system – as well as the simulation of bypass diode faults, in short circuit configuration. A resistor installed inside the QFVG-M allow to increase the string series resistance until 5 Ω to the PV string while connectors directly connected to the Junction Box of two PV modules enable the short circuit of bypass diodes (Fig. 4).

4.3.2 Partial shading

Partial shading effects were simulated by applying artificial shading to the PV modules within the string. This fault condition was designed to replicate scenarios where certain cells in the solar module become closed or blocked [17], as can happen when snow or soiling accumulates on the module, or when objects such as leaves fall onto PV module surface [18]. Depending on the extent of this phenomenon, the resulting impact can vary. Covering 25% of the area of the bottom PV cells may lead to a current mismatch between cells, commonly observed in cases of uneven module soiling or partial shading between PV strings. This scenario could

Table 1. Electrical characteristics of the PV systems used in this study.

PV system name	Type of fault	Strings [#]	Modules per string [#]	BP Diode per Module [#]	V_{mpp} [V]	I_{mpp} [A]	P_{STC} [kW]	V_{oc} [V]	I_{sc} [A]
TFV1	– Ground Fault – R_{iso} Low – Partial shading – Line-to-Line Fault – Bypass Diode (SC) – Series Resistance	2	24	3	454	8.19	7.44	567	8.7
TFV3	– Bypass Diode (SC) – Partial shading – Series Resistance – HotSpot	1	24	3	430	8.17	3.48	532	8.8

DESCRIPTION ACRONYMS

SC: Short Circuit	V_{mpp}: Voltage @max power
R_{iso} Low: Low insulation Resistance	I_{mpp}: Current @max power
BPDiode: Bypass Diode of PV Module	P_{STC}: DC Power @STC

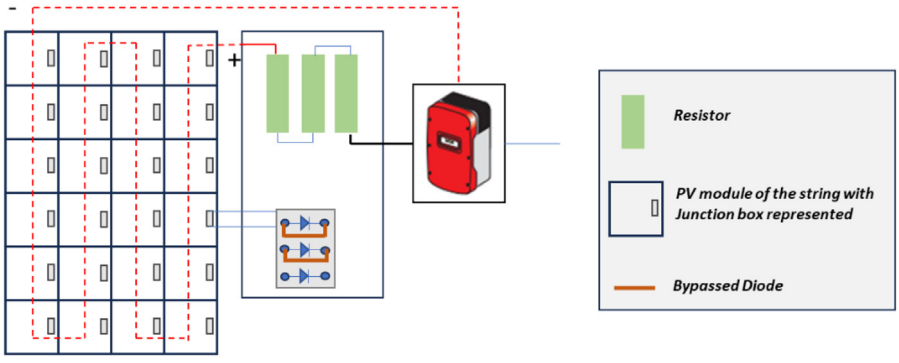

Fig. 4. Diagram of the hardware to replicate Increased Series resistance and shorted bypass diode.

result in a reduction in the current generated by the module or the entire string. When the percentage of coverage increases – we tested until the 50% of the cell area – a complete reduction in string voltage can occur due to the activation of the module's bypass diodes. In our study, a dark cover was used to cover 25% and 50% of the cell of the bottom PV cells of the modules, as illustrated in Figure 5.

4.4 Measurement uncertainty source

Table 2 presents the list of uncertainty sources considered in the measurement of parameters during the PV tests outlined in the following sections.

5 Methodology

5.1 Fault testing program and data collection

The fault datasets analysed in this study were collected between July 1, 2023, and September 2, 2024, covering a period of 429 days. During this time, we generated 673,932 fault-labelled records using the TFV1 and TFV3 systems, including 32,806 records of combined faults (Tabs. 3 and 4). Fault datasets were generated according to a specific testing program designed at the outset of the study. This program alternated between periods of isolated and combined faults. For the analysis of the combined failure mode detailed in this study, both isolated fault periods – where only a single type of malfunction was present – and combined fault periods – where multiple failures occur simultaneously – were examined. The duration of each fault test was determined by the meteorological conditions during the monitoring period and typically lasted no less than one week. For each implemented failure mode, field measurements were conducted using a current–voltage (I–V) curve tracer.

Figure 6 presents an example of the fault testing program used to investigate the effects of single and combined faults on monitored PV data parameters. The numbers within the boxes indicate, depending on the type of fault implemented, the number of diodes, modules, or the resistance values used to emulate the fault conditions.

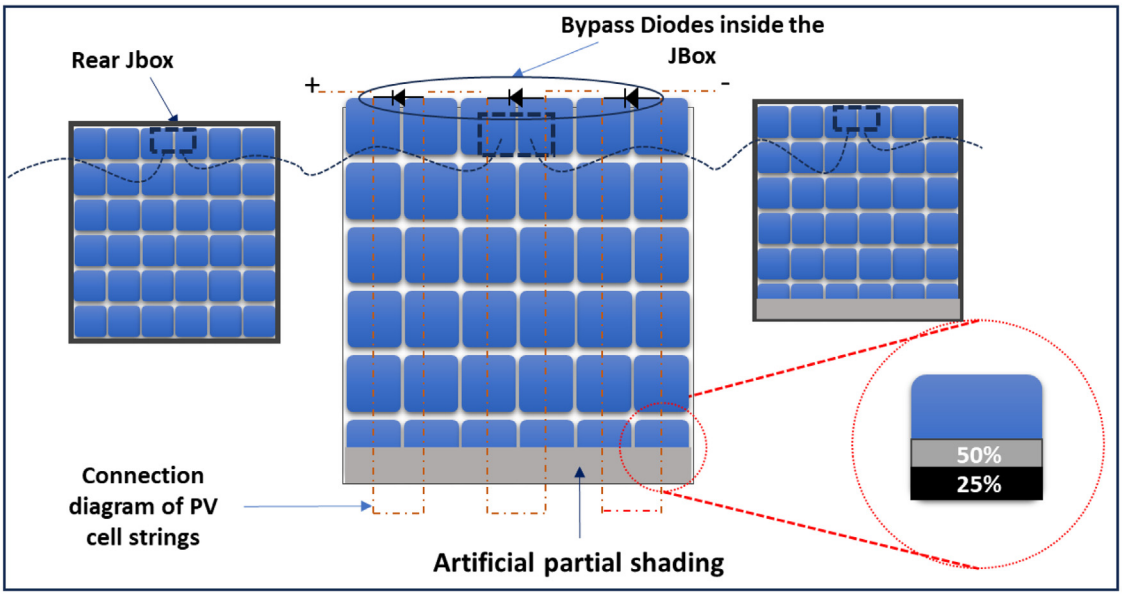

Fig. 5. Illustration of partial shading discussed in this study.

Table 2. List of uncertainty sources considered for the measurements in this study.

Uncertainty sources	U (%)	pdf	k	$u_i = U/k$
Voltage (V)	1	Gaussian	2	0.005
Current (A)	1	Gaussian	2	0.005
Sampling interval (Δt) − CPU clock stability	0.0001	Rectangular	1.75	0.000
Series Resistance (Ω)	0.04	Gaussian	2	0.005

pdf: probability density function; U: Uncertainty; K: factor.

Table 3. List of implemented and analyzed failure in TFV3 and relative records analyzed.

Failure type	Acronym	Number of records labeled with faults	Period of monitoring
Normal Operation − No Failure in the PV String	NO	9,180	From: 13/06/2024 To: 02/09/2024
Four Diode Fault	4DSC	7,875	
Increased Series Resistance @ 5Ω	RS5Ω	10,441	
Four Modules in Partial shading, with 50% cell area covered	4M-PS50	11,522	
Four Diode Fault + Four Modules in Partial shading, with 50% cell area covered	4DSC+ 4M-PS50	14,634	Total days: 81
Four Diode Fault + Increased Series Resistance @ 5Ω	4DSC+RS5Ω	11,932	
Increased Series Resistance @ 5Ω + Four Modules in Partial shading, with 50% cell area covered	RS5Ω +4M-PS50	6,240	
TOTALS		71,824	

Table 4. List of implemented and analyzed failure in TFV1 and relative records analyzed.

Failure type	Acronym	Number of records labeled with faults	Period of monitoring
Normal Operation – No Failure in the PV String	NO	427,078	From: 01/07/2023 To: 31/07/2024
Two Diode Fault	2DSC	35,265	
Four Diode Fault	4DSC	31,470	
Eight Diode Fault	8DSC	39,604	
Increased Series Resistance @1Ω	RS1Ω	23,804	
Increased Series Resistance @2Ω	RS2Ω	19,502	
Increased Series Resistance @3Ω	RS3Ω	10,980	Total days: 395
Two Modules in Partial shading, with 25% cell area covered	2M-PS25	7,086	
Four Modules in Partial shading, with 25% cell area covered	4M-PS25	7,319	
TOTALS		602,108	

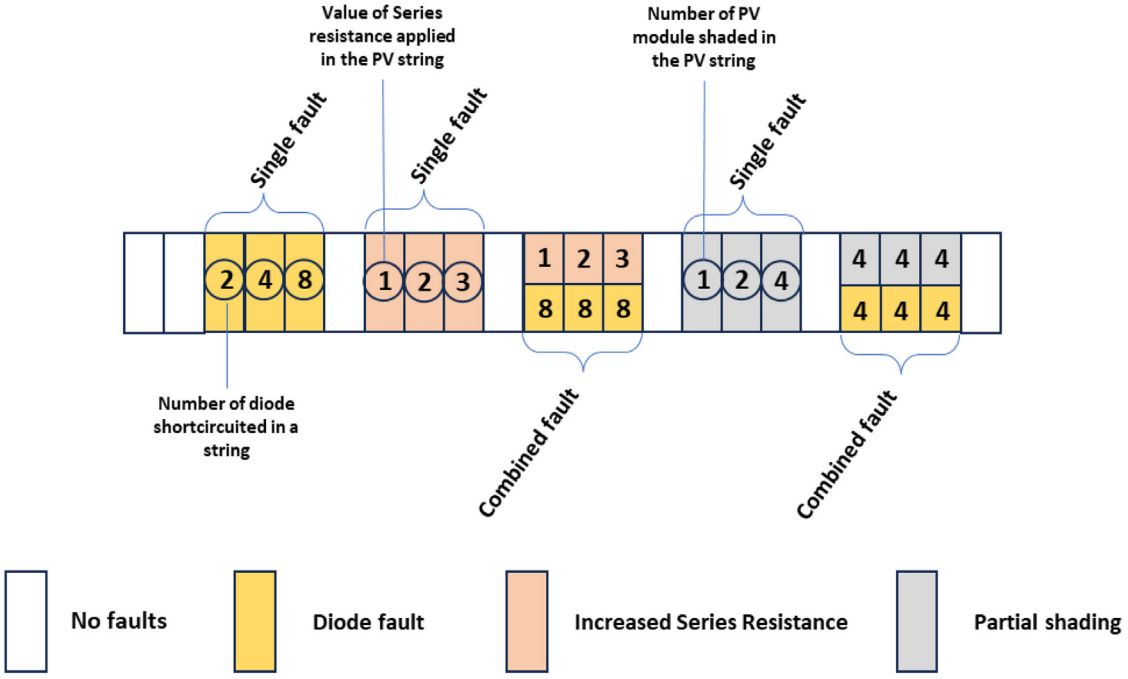

Fig. 6. Example of the fault testing schedule and the implementation modalities of the faults.

5.2 Data analysis processing with *I–V* curve measurement

As previously mentioned, combined faults—malfunctions that occur simultaneously—result in overlapping effects. This overlap makes it challenging for fault diagnostic models to accurately identify and distinguish such faults, leading to reduced diagnostic accuracy i.e. accuracy in fault recognition. The objective of this analysis has been twofold: on the one hand, to characterize the malfunctions through the time analysis of electrical parameters acquired by the monitoring system, attempting to identify distinctive features for each type of fault; on the other hand, to identify the best approach to facilitate their recognition by fault diagnostic models when overlaps occur.

The initial phase of characterizing these faults has involved examining the voltage–current (I–V) characteristic curves for single and combined fault events. For each fault, at least three measurements of the I–V curves were conducted, and their characteristic parameters were analysed, namely the dimensionless ratios:

$$i_r = \frac{I_{mp}}{I_{sc}}, v_r = \frac{V_{mp}}{V_{oc}}, FF = \frac{P_{mp}}{V_{oc} I_{sc}} \quad (1)$$

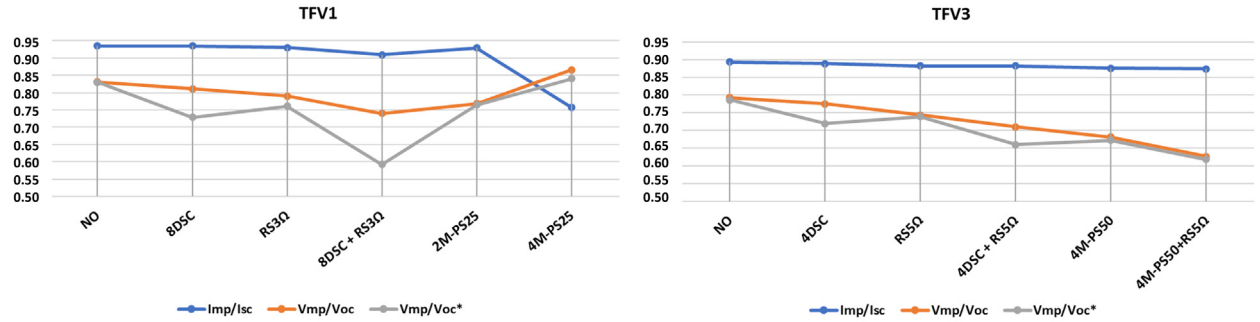

Fig. 7. Effect of short-circuited bypass diode (8DSC), partial shading (4M-PS50) and series resistance (RS5Ω) faults on the i_r and V_r ratios measured in the Current Voltage curve.

where:
- I_{mp} e V_{mp} are the current and voltage at the maximum power point, respectively;
- I_{sc} is the short-circuit current of the string;
- V_{oc} is the open-circuit voltage of the string;
- P_{mp} is the product of I_{mp} and V_{mp} corresponding to the maximum power point of the string.

5.3 Data analysis processing with PV data monitoring

Before initiating the analysis of photovoltaic (PV) data from the SCADA system, an evaluation of data quality to ensure its reliability for fault diagnosis and PV performance monitoring have been conducted. The initial steps in the data pre-conditioning process involve several key operations, including importing the data, assessing its quality.

The data quality check and manipulation procedures encompass routines designed to verify the consistency and completeness of the dataset. These procedures may involve segmenting the dataset into sub-datasets for more manageable analysis. Specific investigations during this phase include:
- Diagnosing missing data, such as NaN (not a number) or NA (not available) values;
- Identifying erroneous values by analysing their distribution or checking for values that fall outside expected physical bounds (e.g., if the recorded power exceeds the nominal power of the PV plant, the data's reliability must be assessed);
- Detecting corrupted data, which might be indicated by anomalous values such as '6000' or '-6000' due to data logger errors;
- Verifying the availability of data for the specific time intervals under analysis.

Following the initial data quality check, the datasets generated from the PV systems undergo a detailed analysis. This analysis ensures that the behaviour of the acquired parameters aligns with the observations made from the I–V curve analysis for the same fault mode.

6 Result and discussion

The failure modes here discussed – short-circuited bypass diodes, increased string series resistance, and partial shading – exhibit similar impacts on PV string voltage, potentially leading to misclassification. We focused our attention on these faults as single effects and in the overlapping of their effects in electrical parameter. The approach taken to address this challenge involves studying the time-dependent behaviour of each fault and identifying methods to uniquely distinguish between different fault types.

6.1 Analysis of *I–V* curves under fault condition

The graph shown in Figure 7 illustrates the two parameters: i_r, v_r derived from the current–voltage (I–V) curves measured in the TFV1 and TFV3 systems under conditions of short-circuited diodes (DSC), module partial shading (M-PS), increased series resistance (RS), and in the absence of faults (NO). The blue line represents the trend of i_r under fault-free period and faulty conditions replicated in the PV system. The orange line represents the v_r ratio, considering the V_{oc} measured during the faulty condition. The grey line is the v_r ratio, considering the open circuit voltage value measured during fault-free periods (indicated as V_{oc}*). As expected, the primary effect of these faults is on the string voltage, conversely, the current value remains nearly constant, regardless of the fault type. This representation confirms the challenges of fault recognition when a reduction in string voltage is observed over a monitoring system. The effect is even more obscured in cases of combined faults, where the primary cause of the voltage drop is linked to multiple issues. The graph v alidates the importance of using the string voltage measured during fault-free periods as a reference parameter for fault observation, as it allows for a more accurate assessment of the fault's severity. This is not essential when investigating the presence of increased series resistance. In that case, the reduction observed using the open-circuit voltage during the fault or fault-free period is equivalent.

Concerning the partial shading phenomena, analysed within the TFV1 system, shading two modules in a string of 24 by covering 25% of the cell area of the bottom PV cells (2M-PS25) led to a reduction in voltage at the maximum power point (MPP). In contrast, applying the same shading to four modules (4M-PS25) caused an increase in MPP voltage, along with a simultaneous reduction in MPP current. This happens because a shaded cell, unable to produce sufficient current, effectively operates as a load,

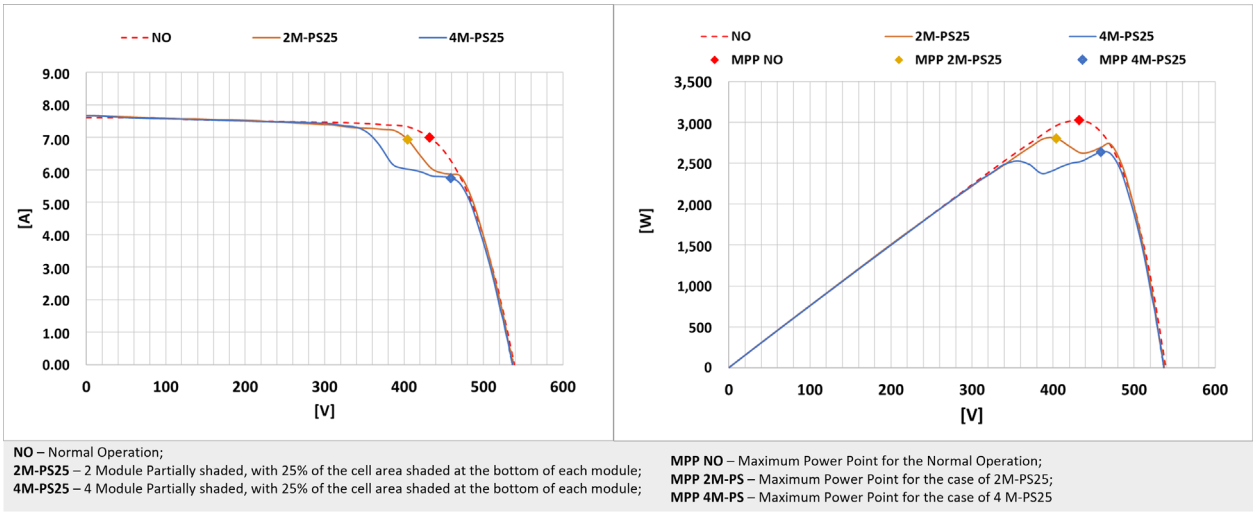

Fig. 8. Measured I–V and P–V curves in the TFV1 system under different partial shading conditions applied to 2 and 4 PV modules. The shading position within the PV string or modules causes a shift in the Maximum Power Point (MPP), mainly impacting the Voltage for the 2M-PS25, and both voltage and current parameters in case of 4M-PS25.

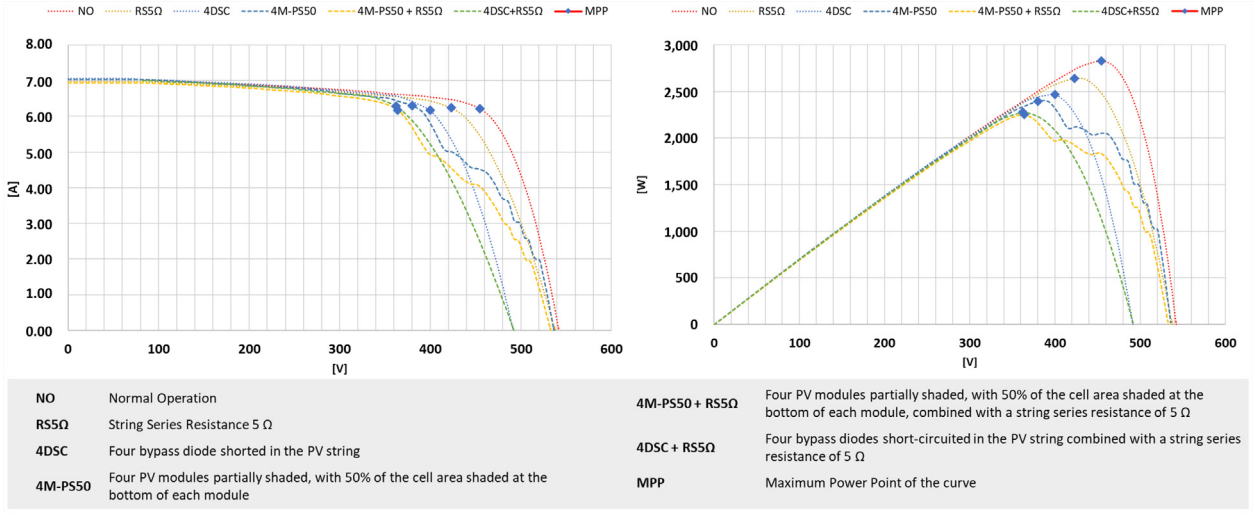

Fig. 9. Measured I–V and P–V curves of the TFV3 system under three distinct failure modes: increased series resistance (5 Ω), partial shading applied to four PV modules, and four bypass diodes shorted; the figure also illustrates scenarios involving combined failure modes.

receiving current generated by other cells in the string. If the reverse voltage across the shaded cell(s) becomes large enough, the BPD connected in anti-parallel activates, causing the I–V curve to exhibit multiple steps.

Figure 8 illustrates the measured I–V and P–V curves for the cases of two (2M-PS25) and four (4M-PS25) partially shaded PV modules, compared to the Normal Operation (NO) condition. The dots on the curves (MPP-NO, MPP-2M-PS25, MPP-4M-PS25) indicate the Maximum Power Point for each operating condition. It is noteworthy that the type of shading—specifically, the number of modules affected by partial shading within the photovoltaic string—differentially impacts the voltage and current at the Maximum Power Point on the I–V curve. Additionally, the P–V curves highlight the reduction in maximum available power under partial shading, with a more significant loss observed for the 4M-PS25 case compared to the 2M-PS25 case.

Figure 9 shows the I–V curves measured from the TFV3 PV system under various replicated failure conditions, including partial shading. Also, in this case the string voltage remain the main parameter affected by these failure modes. A different effect was observed in the TFV3 PV system, where shading was for 50% of the cell area at the bottom of the PV modules (refer to Fig. 5 for illustration). This 50% shading led to the activation of all three bypass diodes, causing a notable reduction in string voltage. Local maximum points are also observed on the P–V curve, which can lead to instability as the inverter tracking algorithm attempts to locate the MPP of the curve of the shaded scenario.

6.2 Analysis of monitored PV data under fault conditions

Observing the failure modes from the IV curve perspective, it confirms that relying solely on output power measurements is insufficient for accurately identifying PV system faults especially when we have to manage their simultaneity. Moreover, due to their similar impacts on string voltage, it becomes essential to process PV monitored data appropriately, taking into account the temporal behavior under different failure modes.

We now examine the approach for handling monitored parameters in fault diagnosis. To eliminate the effects of irradiance and temperature on voltage and current parameters, it is essential to translate the measured values to standard test conditions (STC) using the procedure outlined in the international standard IEC 60891 [19]. The equations used for the correction of current and voltage values are provided below.

$$I_{mpp\_stc} = I_{meas}(1 + \alpha(T_{stc} - T_{mod}))\frac{G_{stc}}{G_{meas}} \tag{2}$$

$$V_{mpp\_stc} = V_{\mathbf{1}} + V_{OC\mathbf{1}}(\beta(T_{stc} - T_{mod})) + \alpha \ln\frac{G_{stc}}{G_{meas}} - R_s^{'}(I_{\mathbf{2}} - I_{\mathbf{1}}) - k'(T_{stc} - T_{mod}) \tag{3}$$

where
- I_{meas}, V_{meas}: represent the measured current and voltage, respectively.
- G_{meas}: measured irradiance on plane of array.
- G_{stc}: reference irradiance of 1000 W/m^2 (Standard Test Condition).
- T_{mod}: the measured temperature of the rear side of the module.
- T_{stc}: the reference temperature, equivalent to 25 °C.
- V_{OC1}: the open-circuit voltage of the string (567 V for TFV1 and 532 V for TFV3 in this study).
- α,β: the PV module temperature coefficients for current and voltage, respectively.
- R'$_s$: the internal series resistance.
- k': resistance temperature coefficient.

For this study, we assumed R'$_s$ to be constant over the period of analysis, since in general the internal series resistance of a photovoltaic module tends to vary little over time, particularly in the absence of physical damage or significant anomalies (such as accelerated material aging). Therefore, we hypothesized that this resistance remained constant throughout the analysis, as no changes were observed in the field measurements, which were taken after each test period to verify the restoration of the operating conditions. We also considered $k' = 0$, because although the series resistance of a photovoltaic module is influenced by temperature, this influence is relatively small compared to other factors, such as the variation in voltage at the maximum power point due to shading conditions and faults applied to the system.

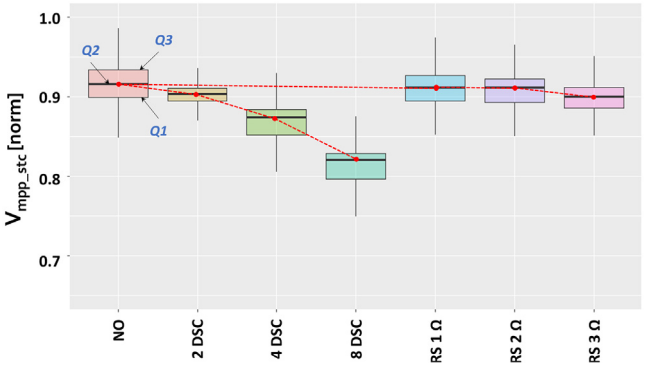

Fig. 10. Analysis of string voltage at the maximum power point as the number of short-circuited diodes and the applied series resistance on the string increase.

The string voltage values, corrected to Standard Test Conditions (STC), are then normalized with respect to the nominal string voltage reference value. Therefore, we have:

$$V_{mpp\_stc[norm]} = \frac{V_{mpp\_stc}}{V_{mpp\_ref}} \tag{4}$$

where V_{mpp_ref} is the nominal string voltage at maximum power point (MPP) of the PV string, obtained as the sum of the nominal MPP voltage values of each PV module, as provided by the module manufacturer.

Figure 10 depicts a box plot comparing the $V_{mpp\_stc[norm]}$ under different fault conditions, considering the production days from 01/07/2023 to 31/07/2024, as summarized in Table 4, and spanning the entire range of irradiance values.

The x-axis represents the scenarios tested: "NO" (normal operation without faults), "2DSC," "4DSC," "8DSC" (indicating an increasing number of short-circuited diodes), and "RS 1 Ω," "RS 2 Ω," and "RS 3 Ω" (indicating increasing series resistance values). The y-axis shows the normalized $V_{mpp\_stc[norm]}$ values, ranging from approximately 0.7 to 1.0. The $V_{mpp\_stc[norm]}$ decreases progressively as the number of short-circuited diodes increases (2DSC, 4DSC, 8DSC). Similarly, the voltage decreases as series resistance (RS) increases. Each box plot illustrates the distribution of normalized $V_{mpp\_stc[norm]}$, with the median values for each condition (see Tab. 5). The red dashed line shows the downward trend of $V_{mpp\_stc[norm]}$ with increasing fault severity (both for DSC and RS scenarios) [20].

Considering the partial shading scenario, in Figure 11 and Table 6 is shown the effect of the 25% shading of the cell area on the lower part of the module (2M-PS25 and 4M-PS25), where, in this case, both, current and voltage monitored values was impacted by the shading condition. When two photovoltaic modules were affected by this phenomenon (2M-PS25), the voltage V_{mpp_stc}, showed

Table 5. Value of the Q1, Q2, Q3 of the boxplot illustrated in Figure 10.

	NO	2 DSC	4 DSC	8 DSC	RS 1Ω	RS 2Ω	RS 3Ω
Q3	0.932	0.909	0.882	0.828	0.925	0.921	0.909
Median (Q2)	0.912	0.902	0.869	0.818	0.909	0.901	0.891
Q1	0.892	0.872	0.840	0.783	0.890	0.886	0.879

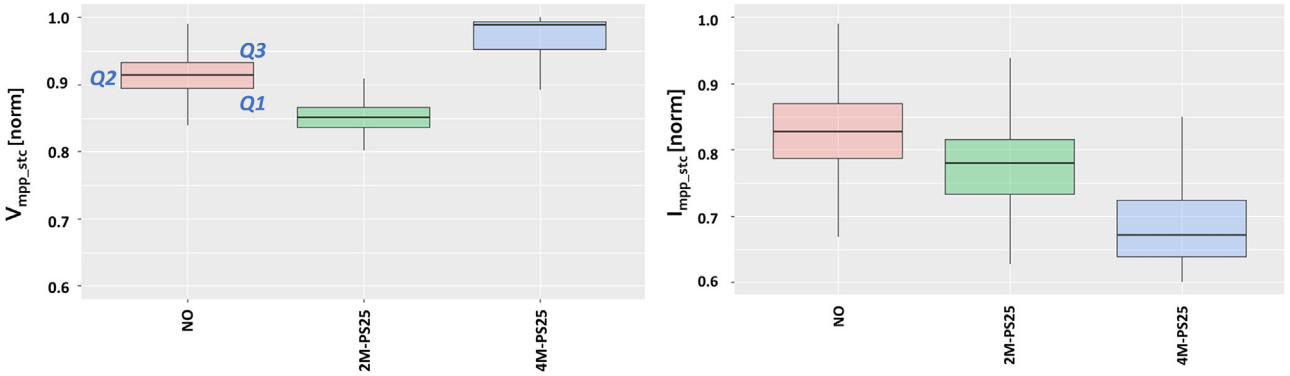

Fig. 11. Normalized value of $V_{mpp\_stc[norm]}$ and $I_{mpp\_stc[norm]}$ showing the impact of 25% shading on the cell area in the lower part of the module. The comparison includes the cases of two shaded modules out of 24 (2M-PS25) and four shaded modules out of 24 (4M-PS25) against the failure scenario (NO).

Table 6. Value of the Q1, Q2, Q3 of the boxplot illustrated in Figure 11.

	$V_{mpp\_stc[norm]}$			$I_{mpp\_stc[norm]}$		
	NO	2M-PS25	4M-PS25	NO	2M-PS25	4M-PS25
Q3	0.936	0.868	0.998	0.871	0.815	0.718
Median (Q2)	0.921	0.851	0.980	0.828	0.777	0.669
Q1	0.902	0.837	0.989	0.786	0.728	0.641

the major decrease, while the string current (I_{mpp_stc}) a slight decrease. This drop in current observed is directly linked to the maximum power point (MPP) of the corresponding IV curve. As illustrated in Figure 8, slight reduction in current may be caused due to the shift in the MPP. When four photovoltaic modules were shaded (4M-PS25), the V_{mpp_stc} exhibited a significant increase, while I_{mpp_stc} showed a notable decrease. Compared to Figure 8, this behaviour can be explained by the fact that at the maximum power point, the I–V curve for the four shaded modules corresponds to a higher voltage and lower current. Naturally, when shading occurs in a PV plant, MPPT tracking algorithms may experience instability while attempting to locate the MPP of the shaded curve. Consequently, the monitored data may inherently include potential errors resulting from the MPPT tracking behaviour of the inverter.

6.3 Analysis of early-morning voltage values under fault conditions

If we were to remotely diagnose the shorted bypass diode, increasing series resistance and partial shading faults, using the monitored PV data, it would be challenging to clearly distinguish the type of fault solely through the analysis of string voltage and current, let alone if we only had the total system power available. To differentiate these faults, we define $\boldsymbol{V^*_{oc,meas}}$ as the voltage values closest to the open-circuit voltage, obtained from the monitoring dataset using the following filters:

– Temperature-corrected voltage (V_{mpp_stc}) values to compensate for thermal effects on the string voltage.
– Low string DC current values ($I_{dc} \ll 0.5$ A).
– Solar irradiance values are between 10 and 100 W/m^2.
– Data acquired between 05:00 and 08:00 each day.

Since the effect of a bypass diode short-circuit fault is independent of irradiation, it is possible to observe a reduction in $V^*_{oc,meas}$, that became more evident with the increasing of the number of shorted bypass diodes. Analysing the $V^*_{oc,meas}$ values in the presence of both faults – increasing series resistance and shorted bypass diode – the $V^*_{oc,meas}$ reveals a clear distinction between the effects of the two fault types (see Fig. 12 and Tab. 7). Specifically, the increased series resistance fault does not significantly affect $V^*_{oc,meas}$, whereas there is a clear linear

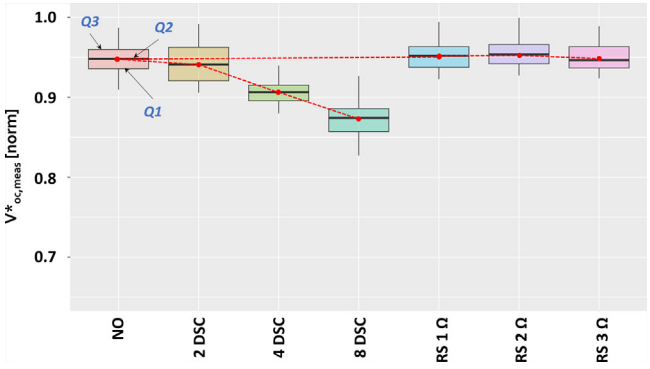

Fig. 12. TFV1: Comparison of $V^*_{oc,meas}$ in the presence of bypass diode failure and string series resistance increase.

Table 7. Value of the Q1, Q2, Q3 of the boxplot illustrated in Figure 12.

	NO	2 DSC	4 DSC	8 DSC	RS 1Ω	RS 2Ω	RS 3Ω
Q3	0.964	0.970	0.921	0.936	0.969	0.969	0.968
Median (Q2)	0.950	0.953	0.908	0.879	0.954	0.956	0.949
Q1	0.936	0.925	0.896	0.862	0.939	0.945	0.937

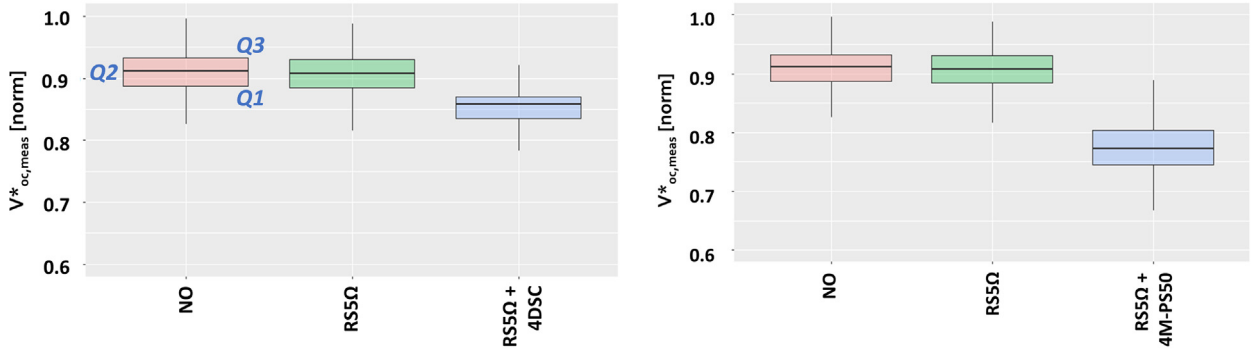

Fig. 13. TFV3 Comparison of $V^*_{oc,meas[norm]}$ in the presence of bypass diode failure, string series resistance increase, and partial shading.

Table 8. Value of the Q1, Q2, Q3 of the boxplot illustrated in Figure 13.

	$V^*_{oc,meas[norm]}$			$V^*_{oc,meas[norm]}$		
	NO	RS5Ω	RS5Ω +4DSC	NO	RS5Ω	RS5Ω+4M-PS50
Q3	0.936	0.934	0.869	0.936	0.934	0.801
Median (Q2)	0.91	0.905	0.858	0.91	0.905	0.768
Q1	0.895	0.895	0.837	0.895	0.895	0.749

relationship between the number of affected bypass diodes and $V^*_{oc,meas}$.

Figure 13 and Table 8 present two box plots displaying data gathered from the TFV3 system, where a series resistance of 5 Ω (RS5Ω) was applied to the string, four bypass diodes were shorted (4DSC), and partial shading was applied to 50% of the cell area in the lower part of four PV modules (4M-PS50). The y-axis represents the $V^*_{oc,meas[norm]}$ values in both plots calculated as:

$$V^*_{oc,meas[norm]} = \frac{V^*_{oc,meas}}{V_{mpp\_ref}}. \quad (5)$$

The normal operation condition without failure (NO) and the increased series resistance conditions (RS5Ω), which show higher values of $V^*_{oc,meas[norm]}$, are consistent

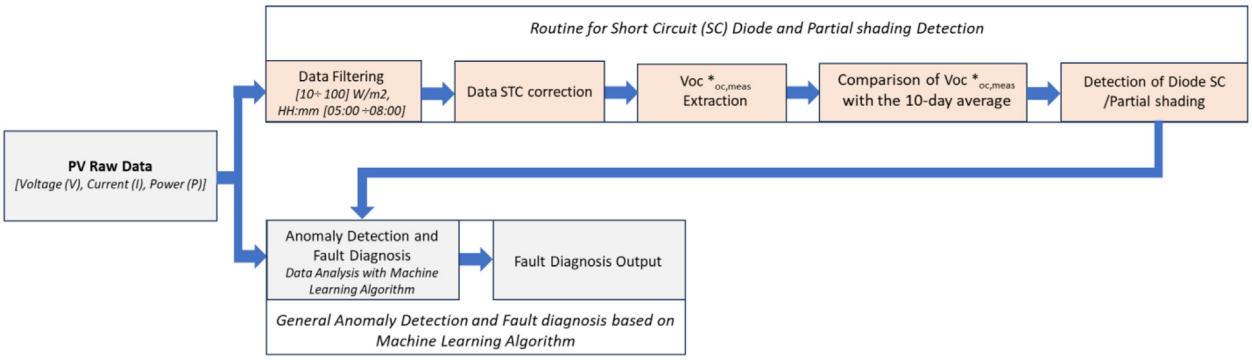

Fig. 14. General flowchart Fault detection and diagnosis.

and comparable. In contrast, under the combined fault conditions (RS5Ω + 4DSC and RS5Ω + 4M-PS50), a significant decrease in string voltage is observed. The increase in series resistance (RS5Ω) has a negligible effect on $V^*_{oc,meas[norm]}$, thus enabling isolation of the fault type to either short-circuited bypass diodes (4DSC) or partial shading (4M-PS50). In this specific case, shading the last row of cells for 50% of the cell area led to the same outcome by triggering the activation of the module's bypass diodes.

The use of Early-Morning Voltage $V^*_{oc,meas[norm]}$ enables differentiation of the underlying cause reducing the voltage of a photovoltaic string. This method can be integrated into fault detection algorithms to distinguish between faults with similar effects, such as diode failure, partial shading, and increased series resistance.

7 Use of early-morning voltage to fault diagnosis algorithm in simultaneous failures

As already mentioned in the introduction, a key limitation of current AI-driven maintenance tools for PV systems lies in their reduced accuracy when multiple faults occur simultaneously. From this study we observed that faults such as increased series resistance, shorted bypass diodes, and partial shading similarly impact PV string voltage. However, their effects can be differentiated by analyzing string voltage during early morning hours, under low irradiation (<100 W/m^2), or prior to inverter grid connection. During this period, voltage drops caused by resistive degradation (e.g., corrosion) remain negligible. In contrast, these parasitic resistance effects become pronounced under moderate irradiation levels (700–900 W/m^2). For partial shading conditions, this study highlights that mismatched cell currents within a PV string can activate all the bypass diodes of a module, significantly affecting string voltage. At 50% shading (4M-PS50), the activation of bypass diodes, caused a substantial reduction in string voltage while in the case of shading of 25% of the cell area in the lower row of cells (2M-PS25 and 4M-PS25), both voltage and current have been impacted.

7.1 Integration with machine learning

The $V^*_{oc,meas}$ analysis, extracted during early morning hours, can be implemented as a standalone routine and seamlessly integrated into Machine Learning (ML) algorithms (Fig. 14). The $V^*_{oc,meas}$ values are compared with the average values acquired with the 10-day and the analysis identify any signs of short-circuited bypass diode faults.

Therefore, this routine can provide a Boolean output for fault diagnosis:

- Boolean 1: Analyzing the $V^*_{oc,meas}$, the voltage drop is likely due to diode short-circuiting (SC) or partial shading.
- Boolean 0: Analyzing the $V^*_{oc,meas}$, no significant early-day voltage drop, suggesting other faults (e.g., increased series resistance) may manifest later.

In cases where $V^*_{oc,meas}$ indicates partial shading/diode SC (Boolean 1), but the ML algorithm identifies a larger voltage drop during the day, the system can diagnose the concurrent presence of multiple faults (e.g., diode SC and increased series resistance). This hybrid methodology improves diagnostic precision and reliability.

The diagnostic process is visualized in Figure 14 and summarized in Table 9.

8 Conclusion

In this study, an innovative methodology was proposed to enhance fault diagnosis capabilities in photovoltaic (PV) systems, particularly under conditions of simultaneous faults. The methodology is based on the analysis of an extensive dataset comprising over 1.6 million fault-labelled records, allowing for a detailed examination of string voltage and current behaviour under three key fault conditions: increased series resistance, short-circuited bypass diodes, and partial shading. These specific faults were chosen because their effects on voltage are similar, making it challenging to accurately diagnose them when they occur concurrently.

The proposed approach leverages an in-depth understanding of the behaviour of voltage and current parameters as these faults manifest throughout the day under varying levels of irradiance. By applying targeted filters to the

Table 9. Diagnostic workflow for fault detection and analysis in photovoltaic (PV) systems, detailing each stage from raw data acquisition to comprehensive fault diagnosis. The integration of early-morning voltage analysis ($V^*_{oc,meas}$) in Machine Learning (ML) algorithms enables differentiation and identification of simultaneous faults such as diode short-circuiting, partial shading, and increased series resistance.

Stage	Description	Output
Stage 1: Data Acquisition	Collection of raw PV data, including voltage (V), current (I), and power (P).	Raw PV dataset
Stage 2: Data Filtering	Filtering data under specific conditions, such as low irradiance (<100 W/m^2) and specific time intervals (05:00–08:00).	Filtered dataset
Stage 3: Data Correction	Applying Standard Test Condition (STC) correction to normalize voltage and current values.	$V^*_{oc,meas}$ under STC
Stage 4: $V^*_{oc,meas}$ Extraction	Extraction of the corrected open-circuit voltage to assess early-day voltage behavior.	Boolean value (0 or 1)
Stage 5: ML Algorithm Input	Input Boolean values from $V^*_{oc,meas}$ routine into the Machine Learning fault detection algorithm.	ML-ready Boolean data
Stage 6: Fault Diagnosis	Using the ML algorithm to diagnose potential faults (e.g., diode SC, partial shading, or increased series resistance).	Fault identification and severity
Stage 7: Multiple Faults Analysis	Cross-analyzing early-day and full-day voltage behavior to diagnose the simultaneous presence of multiple faults.	Comprehensive fault diagnosis

analysed dataset, the results demonstrate that this methodology enables the reliable identification and classification of faults, even in the presence of multiple overlapping malfunctions. This approach is particularly effective in reducing the risk of misdiagnosis, as it enhances the ability of AI-based algorithms to recognize faults in more complex scenarios, such as when simultaneous failures occur.

The proposed methodology provides a robust foundation for further research and practical applications. The integration of the measured open-circuit voltage ($V^*_{oc,meas}$) into fault detection and diagnosis algorithms has the potential to improve the reliability of fault identification. Future experimental efforts will focus on incorporating this methodology into fault detection algorithms, with particular attention to diagnosing combined faults and applying the proposed steps to large PV systems under real operating conditions.

Glossary

Acronym	Description
$V^*_{oc,meas}$	DC Voltage String measured @ DC current values (Idc $\ll$ 0.5 A) and Irradiance between [10–100] W/m^2
$V^*_{oc,meas[norm]}$	The $V^*_{oc,meas}$ normalized, obtained dividing the measured voltage by the nominal string voltage
I_{sc}	Short-circuit current of the PV string modules
AI	Artificial Intelligence
DC	Direct Current
DSC	Diode in short circuit
FF_r	Fill_factor reference calculated from the measured IV Curve
i_r	Current Reference calculated from the measured IV Curve
I_{mpp_stc}	DC String Current corrected @ STC value according to IEC 60891
ML	Machine Learning
MPP	Maximum power point
NA	Not available values.
NaN	Not a number
O&M	Operation & Maintenance
PS	Partial Shading
2M-PS25	Partial shading on 2 PV Modules on a string of 24 Modules, in which the 25% of the area of the bottom PV cells are shaded
4M-PS25	Partial shading on 4 PV Modules on a string of 24 Modules, in which the 25% of the area of the bottom PV cells are shaded
2M-PS50	Partial shading on 2 PV Modules on a string of 24 Modules, in which the 50% of the area of the bottom PV cells are shaded
4M-PS50	Partial shading on 4 PV Modules on a string of 24 Modules, in which the 50% of the area of the bottom PV cells are shaded
PV	Photovoltaic
RdS	Ricerca di Sistema
RS	Series Resistance
RSE	Ricerca sul sistema energetico
TFV1	PV Power System named TFV1
TFV3	PV Power System named TFV3

$V_{\_mp}$	Voltage at the maximum power point, respectively;
$V_{\_oc}$	Open-circuit voltage of the PV string modules
v_r	Voltage Reference calculated from the measured IV Curve
V_{mpp_stc}	DC String Voltage corrected @ STC value according to IEC 60891

Acknowledgments

This work has been financed by the Research Fund for the Italian Electrical System under the Three-Year Research Plan 2022-2024 (DM MITE n. 337, 15.09.2022), in compliance with the Decree of April 16th, 2018.

Funding

This research was funded by Research Fund for the Italian Electrical System.

Conflicts of interest

The authors have nothing to disclose.

Data availability statement

The dataset generated during the current study are available from the corresponding authors on reasonable request.

Author contribution statement

Conceptualization: Giosuè Maugeri, Davide Bombelli, Alessandro Lavelli; Methodology: Giosuè Maugeri; Data Curation: Simone Arrigoni, Giosuè Maugeri, Alessandro Lavelli; Writing – Original Draft Preparation: Giosuè Maugeri; Writing – Review & Editing: All Authors; Supervision: Andrea Rossetti, Marcello Restelli; Project Administration: Salvatore Guastella.

References

1. IEA – International Energy Agency Renewables 2023-Analysis and forecast to 2028, 2024. www.iea.org
2. M. Topic, R. Drozdowski, W. Sinke, Strategic Research and Innovation Agenda (SRIA), 2021. www.etip-pv.eu
3. E.A.S. Filho, B. Müller, N. Holland, C. Reise, K. Kiefer, B. Kollosch, P.J.C. Branco, Practical recommendations for the design of automatic fault detection algorithms based on experiments with field monitoring data, Sol. Energy **244**, 227 (2022)
4. I.U. Khalil, A. Ul-Haq, Y. Mahmoud, M. Jalal, M. Aamir, M.U. Ahsan, K. Mehmood, Comparative analysis of photovoltaic faults and performance evaluation of its detection techniques, IEEE Access **8**, 26676 (2020)
5. M. Köntge, G. Oreski et al., Assessment of Photovoltaic Module Failures in the Field, Report IEA-PVPS T13-09:2017, 2017
6. K. Marc, C.P. Sarah Kurtz, Review of Failures of Photovoltaic Modules, Report IEA-PVPS T13-01:2014 (2014)
7. Y. Zhao, J.d. Palma, J. Mosesian, R. Lyons, B. Lehman, Line-line fault analysis and protection challenges in solar photovoltaic arrays, IEEE Trans. Ind. Electron. **60**, 3784 (2012)
8. E. Diaz-Dorado, J. Cidras, C. Carrillo, Discretized model for partially shaded PV arrays composed of PV panels with overlapping bypass diodes, Sol. Energy **157**, 103 (2017)
9. Z. Alam, L. Khan, Q. Khan, S. Ullah, S. Ahmed, M. Khan, Integrated fault-diagnoses and fault-tolerant MPPT control scheme for a photovoltaic system, in *15th International Conference on Emerging Technologies (ICET)* (IEEE, 2020), pp. 2–5
10. M. Giosuè, D. Bombelli, V. Urciuoli, Validazione degli algoritmi di rilavamento e diagnosi dei guasti FV, analisi della tecnologia bifacciale e dei sistemi di inseguimento solare, Ricerca di Sistema, Milano, PTR 2019-2021, 2021
11. CEI EN IEC 60812-Failure modes and effects analysis (FMEA and FMECA), 2018
12. K. Abdulmawjood, S. Refaat, M. Walid, Detection and prediction of faults in photovoltaic arrays: a review, in *2018 IEEE 12th International Conference on Compatibility, Power Electronics and Power Engineering (CPE-POWERENG 2018)* (Doha, Qatar, 2018), pp. 1–8
13. E. Garoudja, F. Harrou, Y. Sun, K. Kara, A. Chouder, S. Silvestre, Statistical fault detection in photovoltaic systems, Sol. Energy **150**, 485 (2017)
14. IEC 61730-1-Photovoltaic (PV) module safety qualification – Part 1: Requirements for construction, IEC (2023)
15. IEC 60364-7-712-Low voltage electrical installations – Part 7-712: Requirements for special installations or locations – Solar photovoltaic (PV) power supply systems, IEC (2017)
16. G. Maugeri, R. Andrea, U. Vittorio, B. Davide, S. Guastella, A facility test to generate data from real PV systems affected by faults, in *WCPEC-8, the 8th World Conference on Photovoltaic* (Milan, Italy, 2022)
17. A. Giyantara, Analysis of partial shading effect on solar panel, J. Phys. **012022**, 1726 (2021)
18. N. Kumari, S. Singh, S. Kumar, Performance analysis of partially shaded high-efficiency mono PERC/mono crystalline PV module under indoor and environmental conditions, Sci. Rep. **14**, 21587 (2024)
19. IEC60891-Photovoltaic devices – Procedures for temperature and irradiance corrections to measured *I-V* characteristics (2021)
20. G. Spagnuolo, H. Kalliojärvi-Viljakainen, Identification of series resistance from the measured pv panel electrical characteristics, in *36th European Photovoltaic Solar Energy Conference and Exhibition* (2019)

Cite this article as: Giosue' Maugeri, Simone Arrigoni, Alessandro Lavelli, Davide Bombelli, Salvatore Guastella, Andrea Rossetti, Marcello Restelli, Enhancing fault diagnosis in photovoltaic plants: managing the simultaneity of faulty bypass diodes, series resistance increases, and partial shading effects, EPJ Photovoltaics **16**, 14 (2025), https://doi.org/10.1051/epjpv/2025001